EFFECT OF xBi_2O_3 AND $xTiO_2$ ON THE PHOTOPYROELECTRIC SPECTROSCOPY PARAMETERS FOR ZNO DOPED WITH $1.0MnO_2$ AND $0.4CO_3O_4$

N. NASIR[a], M. KASHIF[b], N. SABIR[b], R. QINDEL[c], Z. RIZWAN[a,*]
[a]*Department of Applied Sciences, Faculty of Science, National Textile University, Faisalabad, Pakistan*
[b]*Department of Physics, G.C University, Faisalabad, Pakistan*
[c]*Department of Physics and Astronomy, King Saud University, Riyadh, Saudi Arabia*

Optical and electrical properties is studied for (ZnO + $01MnO_2$ + $0.4Co_3O_4$ + xBi_2O_3 + $yTiO_2$), where (x=0.6,1 & y=0.6,1mol%) using Photopyroelectric (PPE) spectroscopy that is nondestructive tool, incident light wavelength, kept in the range 300 nm–800 nm modulated at 10 Hz. The main objective of this study is to discuss the PPE spectrum based on doping level and sintering temperature. Optical energy band-gap (E_g) for x=0.6 and 1 mol% is 2.15 eV and 2.17 eV, respectively, which is calculated from the plot $(\rho h\upsilon)^2$ *versus* $h\upsilon$ at 1 hour sintering time. Steepness factor 'σA' and 'σB', is discussed with reference to the variation of E_g and sintering time which describe the slope of exponential+l optical absorption. Other characterization for the ceramic were studied using XRD, EDAX and SEM. The relative density decreased with the increase of sintering time and doping level. It was investigated that the grain size increased with the increase of sintering time.

(Received August 24, 2020; Accepted November 27, 2020)

Keywords: PPE Spectroscopy, ZnO, Electrical properties

1. Introduction

Gas sensors of ZnO based ceramic semiconductors are widely used, for piezoelectric, solar cells electrodes, phosphors, varistors and transparent conducting films [1-3]. It is wide band gap ceramic [4]. High energy absorption capability verses various surges is possessed by the Varistors. Unwanted magnitudes of the transient voltage surges is regulated if they are widely used as protecting devices. This is caused by their fast response over voltage transients. Varistors can detect in nanosecond speed and clamp transient voltage pulses. The particular role of numerous additives is uncertain in the electronic structure of ZnO based varistors. Extensive research of ZnO varistors based on the improvement the electrical properties is continued [5]. The most important parameter is high non-linear characteristics to be considered for the formulation of varistors. Small quantities of other metal oxides such as aluminum oxide, cobalt oxide, bismuth oxide etc. are used to form Varistors [5]. The stability and non-linear response of the varistor is improved using such additives as the main tools. The procedure regarding the grain boundaries and related fault concentration gradients can be the explained by nonlinear response [5]. Impurities and their behavior, the distribution of vacancies, depend on electrical properties for ZnO based ceramic. In previous studies, extensive research work on voltage, current characterization of ZnO varistors have been done. It is vital for the analysis of electronic states to get the behavior of optical absorption of Zinc oxide ceramic doped with metal oxides. Doping level of MnO_2 and Co_3O_4 with variable doping level of Bi_2O_3 and TiO_2 at different sintering times has been discussed in the context of Optical and electrical parameters.

* Corresponding author: zahidrizwan64@gmail.com

2. Materials and methods

Zinc Oxide (Alfa Aesar, 99.9% pure) with 1 MnO2 (Alfa Aesar, 99.999% pure), 0.4Co2O3 (Alfa Aesar, 99.7% pure) and $xBi_2O_3 + yTiO_2$ (Alfa Aesar, 99.6% purity,) was doped with (x=0.6, 1 & y=0.6, 1mol%). Powder samples of all elements of each mole percent was pre-sintered at rate of 4 °C/min (heating and cooling) in open atmosphere at 700 °C for 120 minutes. PVA (1.2 wt %) was mixed as a binder after the samples were crushed to bind the sample. The dried powder with a force (760 kg cm^{-2}) was pressed to make a disk (10 mm) diameter. The disks were sintered for (1- 4 h) with one hour interval for each sample at 1260 °C at the heating and cooling rate of 3.75 °C min^{-1} in air. The disk from each sample was ground for 45 minutes for X-ray diffraction (XRD) and the photopyroelectric (PPE) spectroscopy analysis. It was granulated by sieving through a 75-mesh screen. Geometrical method is used to calculate the density of the disks [6]). For microstructure analysis polished samples were thermally etched. The grain boundary crossing method is used to determine the Grain size. X'Pert High Score software is used to analyze XRD data.

Signal amplitude has been described for the measurement of PPE. The light beam of the wavelength (300 to 800 nm) was used for PPE measurements at 10 Hz. The excitation photon energy ($h\upsilon$) is the key factor for Optical absorption coefficient (β) variation [7-8], which is given below,

$$(\beta h\upsilon)^2 = (h\upsilon - Eg) \tag{1}$$

Photopyroelectric signal intensity (ρ) is directly related to (β). The quantity $(\rho h\upsilon)^2$ is related to Photon energy ($h\upsilon$) linearly. From the plot of $(\rho h\upsilon)^2$ *versus* $h\upsilon$, the energy band gap is obtained by extrapolating the linear fitted region to zero [9-12].

$$P = P_o e^{\left(\frac{\sigma(h\upsilon - h\upsilon_o)}{KT}\right)} \tag{2}$$

In a diversity of amorphous and crystalline materials the light absorption edge has been detected. The light-immersion edge has a vital role in electron interactions. Signal intensities plotted semi logarithmically which is lesser than the fundamental absorption edge. This varies linearly with the photon energy of PPE [13]. The relation is given by the equation (1, 2) for photon energy and absolute measuring temperature (T) ($h\upsilon$). $P0$, σ, $\upsilon 0$ are fitting parameters, where k is the Boltzmann constant [14-15]. The exponential slope is determined by the value σ/kT. Factor σ which is described in optical absorption edge is the steepness factor. From the PPE spectrum the steepness factor is found (σA in region-A and σB in region-B). The value of barrier height (ϕ_B) can be found in different textbooks [16-17] and in a variety of papers [18-19].

3. Results and discussion

The main phase observed in the XRD analysis for the combination (ZnO +1 MnO_2 + 0.4 Co_3O_4 + 0.6 Bi_2O_3 + 0.6 TiO_2) is ZnO with some other secondary phases as Bi_2O_3 (ref. code 00-018-0244) is detected for the 1 and 2 hours of sintering time. The combination (ZnO +1.0 MnO_2 + 0.4 Co_3O_4+1 Bi_2O_3 +1TiO_2) with the higher additives of Bi_2O_3 and TiO_2 also shows that the secondary phases are development. Small peaks of the Bi_2O_3 (ref. code 100-002-101) was detected for the 1 and 2 hour sintering time. Secondary phases Mn_2TiO_4 and $Zn_2Ti_3O_8$ are found in the ceramic for 3 and 4 hour sintering time, respectively. Two very small peaks of the secondary phase Mn_2TiO_4 (ref. code 00-019-0975) are detected for 3 hour sintering time. Secondary phase Zn_2TiO_4 (ref. code 00-039-0190) is also present for the 4 hour sintering time. Relative density of the ceramic decreases from 88.7 % with the increase of the sintering time and it becomes 88.4% for 4 hour sintering time for the ceramic 1 Bi_2O_3+ 1 TiO_2 combination Fig. 1. When the doping level is decreased as 0.6 mol% of Bi_2O_3 and TiO_2 combination, the density decreases from 89.4 % to 88.9 %. This indicates that the pores increasing with the increase of

sintering time. It is also investigated that the overall density is low about 1.3 % at the higher doping level of Bi_2O_3 and TiO_2 at all sintering times. The increase of sintering time increases Grain size of the ceramics, Fig. 2. Grain size increased from 41 to 77.6 µm with the increase of sintering time for the ceramic 0.6 Bi_2O_3+ 0.6 TiO_2 combinations. This increase is linear in the grain size which increases with the increase of sintering time. This indicates that the grain size increases due to the grain enhancer Bi_2O_3 and TiO_2 already present in this combination as TiO_2 is a strong grain enhancer. When the doping level is changed to 1 mol% of Bi_2O_3 and TiO_2 then the grain size is 46.7 µm and is increased to 74 µm for 3 hour sintering time. But the overall trend in the grain growth is increasing. It is observed that the small grains and abnormal grains, some needle like grains are present in the ceramics at higher sintering temperature as compared to the low sintering temperatures. Energy dispersive X-ray analysis results indicates that the Bi_2O_3 is segregated at the grain boundaries. It was observed that the Mn and Co, Ti is present in the grains indicating the substitution in the ZnO lattice.

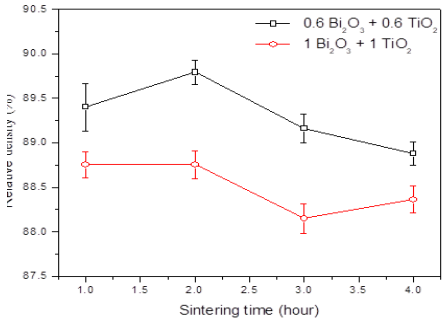

Fig. 1. Variation of density with sintering time.

The energy band-gap (E_g) of the ceramic ZnO is reduced from 3.2 to 2.15 ± 0.01 for the 0.6 Bi_2O_3 + 0.6 TiO_2 ceramic combinations for 1 hour sintering time Fig. 3. This decrease is due to the interface states produced by the combined effect of 0.4 Co_3O_4, 0.6 Bi_2O_3, 0.6 TiO_2 and 1MnO_2. No increase or decrease is observed when the sintering time is increased from 1 to 4 hour sintering time. The value of E_g is constant at about 2.15 ± 0.014 eV for 2, 3, 4 hour sintering time, Fig. 3. For 1 hour sintering time E_g decreases from 3.2 to 2.17 ± 0.01 eV when the amount of additives Bi_2O_3 and TiO_2 is increased from 0.6 to 1 mol%, the ceramic combination becomes as ZnO + 1MnO_2 + 0.4 Co_3O_4 + 1 Bi_2O_3 + 1 TiO_2,. E_g is about constant at 2.15 ± 0.01 eV for the 2 and 3 hour sintering time. The interface states produced by the combined effect of 1MnO_2, 0.4 Co_3O_4, 0.6 Bi_2O_3, 0.6 TiO_2 is the reason for this decrement in energy band gap. The steepness factor σ_A, Fig. 4, slightly increases with the increase of sintering time indicating the decrease in the PPE signal intensity in the ceramics having 0.6 Bi_2O_3+ 0.6 TiO_2 additives [20]. This indicates the increase in the structural ordering. This structural ordering corresponds to the decrease in the interface states.

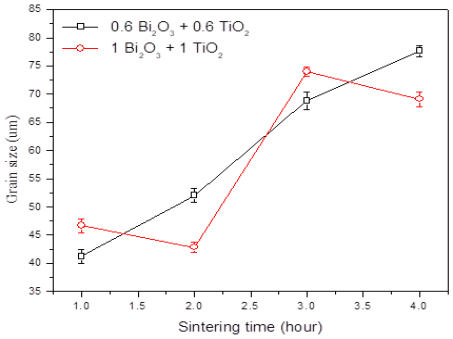

Fig. 2. Variation of grain size with sintering time.

So this decrease in the interface states is not giving very clear increase in the value of E_g but E_g seems slightly increases. The value of σ_A is decreasing very slowly with the and up to 3-hour sintering time and then slightly reduces at the 4 hour sintering time when the additives are increased from 0.6 to 1 mol%. Again, the variation in the value of E_g was not observed clearly but E_g decreases due to the growth of interface states [21]. The steepness factor σ_B increases with the increases slightly with the sintering time indicating the decrease in the average thermal displacement of atoms for the combinations 0.6 Bi_2O_3+ 0.6 TiO_2 and decreases for 1 Bi_2O_3+ 1 TiO_2 , Fig. 5 . This indicates the increase in structural ordering [22]. So due to the increase in structural ordering, interface states decrease and the decrease in the value of E_g increases slightly and case is inverse for 1 mol% doping level.

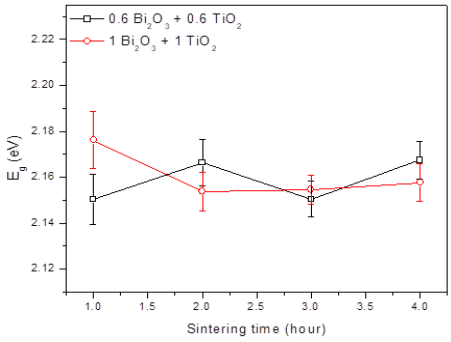

Fig. 3. Variation of E_g with sintering time.

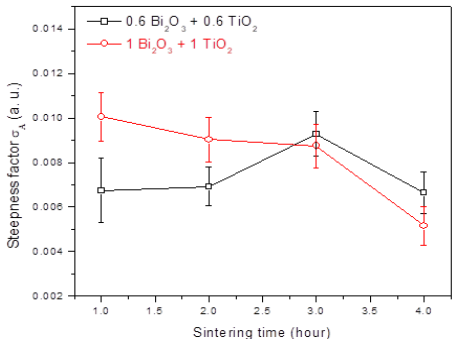

Fig. 4. Effect of sintering time on steepness factor σ_A.

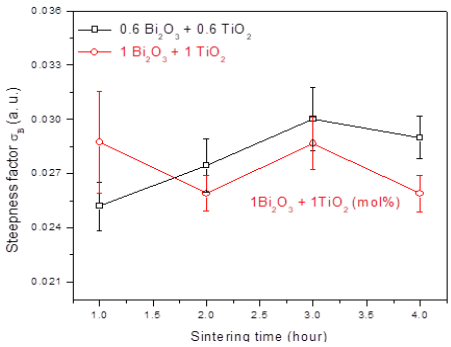

Fig. 5. Effect of sintering time on steepness factor σ_B.

Varistor voltage decreases from 1641 to 1068 V/cm for the ceramic combination 0.6 Bi_2O_3+ 0.6 TiO_2 with the increase of the sintering time. It is related to the grain size as grain size increases, varistor voltage decreases as the number of grain boundaries decreases. Varistor voltage decreases from 1472 to 1064 V/cm with the increase of the sintering time for the ceramic combination 1 Bi_2O_3+ 1 TiO_2. From the current-voltage characteristics, the value of nonlinear coefficient (α) has the value 5, 13.6 at 1, 2 hour sintering time and then decreases to 5.38 with the increase of the sintering time for the ceramic combination of 0.6 Bi_2O_3+ 0.6 TiO_2. When the amount of additives is increased then the value of the nonlinear coefficient is maximum. 6.38 for the sintering time of 1 hour and further increase of the sintering time, nonlinear coefficient decreases slightly. The barrier height, Fig. 6, is decreasing from 0.94 to 0.87 eV with the increase of the sintering temperature for the ceramic combination 0.6 Bi_2O_3+ 0.6 TiO_2. Its value is also decreasing from 0.94 to 0.89 eV with the increase of the sintering time for the combination 1 Bi_2O_3+ 1 TiO_2. The value of barrier height is higher with the lower amount of additives at all sintering times. Dielectric constant, Fig. 7, at 1 KHz, increases from 293 to 2587 with the increase of sintering time for the ceramic combination 0.6 Bi_2O_3+ 0.6 TiO_2. Its value increases from 396 to 1712 with the increase of sintering time for the ceramic combination 1 Bi_2O_3+ 1 TiO_2. This can be directly related to the grain size as $\varepsilon_{app.} = \varepsilon_g$ (d/t). It is found that with the increase of sintering time the value of dissipation factor (Tanδ) increases. This indicates the joule heating loss by leakage current and friction heating loss by electric dipole rotation is increased (Deby 1929-18, Deby 1945-19). Fig. 8. Its value is lower at the higher combination of additives.

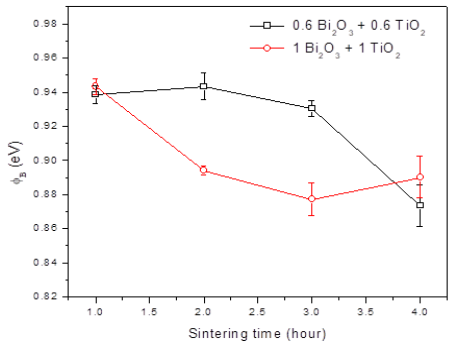

Fig. 6. Variation of barrier height with sintering time.

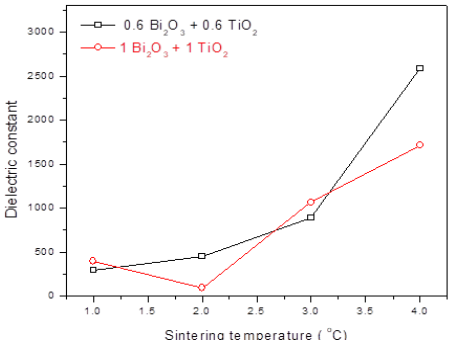

Fig. 7. Variation of dielectric constant with sintering time.

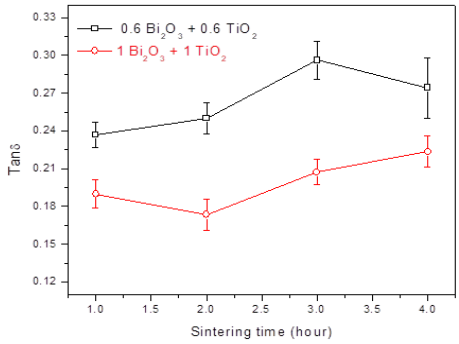

Fig. 8. Variation of dissipation factor with the increase of sintering temperature.

4. Conclusions

The hexagonal phase of ZnO is confirmed by XRD but secondary phases Mn_2TiO_4 and $Zn_2Ti_3O_8$, Mn_2TiO_4, Zn_2TiO_4 are found in the ceramic for 3 and 4 hour sintering time, respectively. Energy dispersive X-ray (EDAX) results indicates that the Bi_2O_3 is segregated at the grain boundaries and the Mn and Co, Ti is present in the grains. The grain size increases from 46.7 and 77.6 μm with the increase of sintering temperature. The relative density decreased slightly with the increase of sintering time and doping level. The optical energy band-gap varies between 2.15 to 2.17 at all sintering temperatures. To study the optical absorption behavior along with the other electrical measurements of ZnO based varistors PPE spectrometry proved to be a useful tool.

References

[1] D. Tamilsel, N. Velman, K. Rathide, Journal of Ovonic Research **16**(2), 123 (2020).
[2] B. Rajesh Kumar, B. Hymavathi, T. Subba Rao, Journal of Science: Advanced Materials and Devices **3**, 433 (2018).
[3] M. I. A. Bhatti, A. Ashara, A. Maryam, Q. Hassan, M. Iqbal, Journal of Materials Research and Technology **9**(3), 4218 (2020).
[4] M. Javed, S. Hussain, Digest Journal of Nanomaterials and Biostructures **15**(1), 217 (2020).
[5] P. Menga, C. Yuana, H. Xub, S. Wanb, Q. Xiec, J. Hec, H. Zhaod, J. Hua, J. Hea, Electric Power Systems Research **178**, 106041 (2020).
[6] W. N. Choon, Material Chemistry and Physics **82**, 157 (2003).
[7] H. Ali, A. M. Alsmadi, B. Salameh, M. Mathai, M. Shatnawi, N. M. A. Hadia, E. M. M. Ibrahim, Journal of Alloys and Compounds, in press (2020).
[8] R. O. Rivas, F. D. Flores, S. A. M. Hernández, J. Q. Galvan, A. Centeno, A. S. Domínguez, J. S. Cruz, Chalcogenide Letters **17**(7), 329 (2020).
[9] L. Akbar, K. Ali, M. Sajjad, A. Sattar, B. Saleem, U. Amjad, A. Rizwan, S. Sehar, W. Akram, M. Tahir, M. Usama, Digest Journal of Nanomaterials and Biostructures **15**(2), 329 (2020).
[10] D. Bekkar, Y. Meftah, B. Benhaoua, A. Rahal, A. Benhaoua, A. H. Hamzaoui, Journal of Optoelectronic and Biomedical Materials **12**(2), 33 (2020).
[11] A. Bagawi, Journal of Non-Oxide Glasses **12**(1), 01 (2020).
[12] A. F. Abdulrahman, Journal of Ovonic Research **16**(3), 181 (2020).
[13] F. Urbach, Physical. Review **92**, 1324 (1953).
[14] J. D. Dow, D. Redfield, Physical Review B **5**, 594 (1972).
[15] S. Qing, T. Toyoda, Japanese Journal of Applied Physics **38**, 3163 (1999).
[16] S. M. Sze, Physics of Semiconductor Devices. Wiley, New York. (1969).
[17] T. K. Gupta, Engineered Materials Handbook, Ceramics and Glasses. ASM Publications **4**, 1150 (1991).
[18] J. Y. W. Seto, Journal of Applied Physics **46**(12), 5247 (1975).
[19] M. Matsuoka, Japanese Journal of Applied Physics **10**(6), 736 (1971).

[20] T. Toyoda, H. Fujimoto, T. Konaka, Japanese Journal of Physics **18**, 3292 (1997).
[21] T. Toyoda, S. Shimamoto, Japanese Journal of Physics **36**, 7257 (1997).
[22] T. Toyoda, S. Shimamoto, Japanese Journal of Physics **37**, 2827 (1998).